Hierarchical Electrode Design of Highly Efficient and Stable Unitized Regenerative Fuel Cells (URFCs) for Long-term Energy Storage

Xiong Peng[1], Zachary Taie[1,2], Jiangjin Liu[1], Yaqian Zhang[3,4], Xinxing Peng[3], Yagya N. Regmi[1], Julie C. Fornaciari[1,5], Christopher Capuano[6], Dustin Binny[7], Nancy N. Kariuki[8], Deborah J. Myers[8], Mary C. Scott[3,4], Adam Z. Weber[1], Nemanja Danilovic[1,*]

[1] Energy Storage and Distributed Resources Division, Lawrence Berkeley National Laboratory, Berkeley, CA, 94720, USA

[2] Oregon State University, School of Mechanical, Industrial, and Manufacturing Engineering, Bend, OR, 97701, USA

[3] National Center for Electron Microscopy, Molecular Foundry, Lawrence Berkeley National Laboratory, Berkeley, CA, 94720, USA

[4] Departments of Materials Science and Engineering, University of California Berkeley, Berkeley, CA, 94720, USA

[5] Departments of Chemical Engineering, University of California Berkeley, Berkeley, CA, 94720, USA

[6] Nel Hydrogen/Proton Onsite, Wallingford, CT, 06492, USA

[7] Ballard Power Systems, Burnaby, British Columbia, V3N 5G2, Canada

[8] Chemical Sciences and Engineering Division, Argonne National Laboratory, Lemont, IL, 60439, USA

[*] Corresponding author: ndanilovic@lbl.gov

Broader context

Electrochemical energy storage devices have the potential to provide clean and sustainable solutions to grid and transportations applications. A proton exchange membrane based unitized regenerative fuel cell (PEM-URFC), which combines a hydrogen fuel cell and water electrolyzer into a unitized device, can specifically target long-term (> 8h) energy storage. However, the widespread application of PEM-URFC has been hindered due to its low round trip efficiencies and poor stabilities – not because of catalysis or ionic conduction, but mainly due to poorly understood and controlled electrode structure, which directly impacts catalyst utilization and mass transport behavior of URFC. This work studies two important electrode parameters including porosity and tortuosity to show the importance of electrode design can help enhance catalyst utilizations and minimize mass transport, which allows us to achieve PEM-URFC with RTEs at 56% and 53% under constant electrode and constant gas mode operation, respectively, more importantly, a stable operation for more than 500 h, making an huge advancement to the field of URFC. This electrode design strategy can also be transferred to other electrochemical devices for energy storage and conversion applications (Zinc-air battery, flow batteries, CO_2 electrolyzer *et.al*).

Abstract

The unitized regenerative fuel cell (URFC) is a promising electrochemical device for intermittent renewable energy storage in chemical bonds. However, widespread application has been hindered due to low round-trip efficiencies (RTEs) and disappointing durability, in particular at high rates. Here, we breakthrough that barrier by demonstrating highly efficient, flexible, and stable URFCs via hierarchical design of the multiscale catalyst-layer structures. A more porous and less tortuous Pt and Ir catalyst layer is realized using a doctor blade fabrication method that significantly improves URFC performance. We demonstrate RTEs of 56% and 53% under constant-electrode and constant-gas mode, respectively, while operating at 1000 mA cm^{-2}, and significantly, an RTE of 45% at 2000 mA cm^{-2}, achievements that were previously viewed as unfeasible under the onerous demands of URFC operation. While at the same time we demonstrate URFCs under both constant-electrode and constant-gas mode operated continuously for over 500 h with negligible degradation. These results demonstrate the viability of applying URFCs for long-term energy storage at previously unattainable efficiencies and cast new light on electrode design and optimization of URFCs.

Introduction

Over the last few decades, global energy demand and consumption has been rapidly growing, and is projected to continue with industrialization and population growth.[1] Environmental concerns such as climate change, air pollution, and greenhouse-gas emissions are limiting further usage of fossil fuels and emphasizing the importance of deploying renewable energy technologies.[2,3] A prominent example of this trend is the increasing deployment of wind, solar, and other renewable electrical generators. These technologies accounted for 45% of new electricity generation in 2018;[4] however, their availability varies substantially not just on a daily cycle but over weekly, monthly, and seasonal periods in most of the populated regions of the world.[5] Due to the intrinsic intermittency, relying on very high shares of wind or solar to achieve deep decarbonization requires overbuilding their total capacity, which leads to high curtailed (wasted) energy and low total capacity utilization rates.[5] Although "firm" electricity generators[6] could help mitigate this problem, they would suffer from low utilization during high renewable-electricity seasons, in addition to still producing CO_2 during operation. Therefore, if one would propose to achieve near zero carbon emission and a strongly reliable electric-power sector, energy-storage technologies capable of sustained input/output over long duration (weeks, months, or even longer) and with high flexibility are urgently needed.

Electrochemical energy-storage technologies offer several unique features, including emission-free operation, compactness and scalability without geographic constraints, and flexible operation profiles to meet different grid demands.[7] The levelized

cost of storage (LCOS) analysis also projects a superiority of electrochemical devices for future electricity-storage solutions.[8] While lithium-ion batteries are the most promising electrochemical devices for short-term (hourly or daily) energy storage, they are less competitive for long-term (weekly or monthly) energy-storage applications[8] due to self-discharge, durability concerns at deep cycling, and high capital cost for long storage times since the storage and conversion functionalities are intimately coupled in a single architecture.[9,10] Redox-flow batteries (RFBs) are also proposed as an alternative choice. Although RFBs do achieve separation of power and energy, they have limitations in low specific energy density due to use of liquid electrolytes, relatively low power densities as well as charge-carrier crossover resulting in loss of charge storage overtime.[11–13] Discrete and unitized regenerative fuel cells (RFCs and URFCs, respectively) could potentially overcome these deficiencies and offer a viable long-term energy-storage solution. Due to the decoupled energy-storage capacity with rated power, RFCs and URFCs mostly avoid self-discharge and do not necessarily have either a linear cost/stored-energy scaling relationship or durability concerns under deep charge/discharge compared to secondary batteries. Importantly, combining a fuel cell and electrolyzer into one unitized electrochemical device accomplishes a compact design with shared balance of plant and cell components, that offers a more economical LCOS compared to discrete reversible fuel cells.[14] A key requirement though is for the URFC to offer comparable high power, energy densities and durability to discrete fuel cells and electrolyzers, which is a challenge we address in this work.

Depending on the conducting electrolyte and operating temperature, URFCs can be classified into high-temperature unitized regenerative solid-oxide fuel cells,[15–18] intermediate-temperature unitized regenerative protonic-ceramic fuel cells,[19–21] low-temperature hydroxide-exchange membrane unitized regenerative fuel cells (HEM-URFCs)[22] and low-temperature proton exchange membrane unitized regenerative fuel cells (PEM-URFCs),[23,24] which are the most promising. Compared to high-temperature (600 – 900°C) or intermediate-temperature (500 – 600°C) URFCs, PEM-URFCs operate under mild reaction conditions, *i.e.* 20 to 100°C and moderate pressure, which could avoid mechanical and chemical compatibility issues for main cell components.[25] Furthermore, PEM-URFCs can rapidly start-up/shut-down and load follows,[26] giving more flexibility in terms of practical operation for grid balancing. Compared to HEM-URFCs or other alkaline based fuel cells[27–32], PEM-URFCs have higher performance and better durability, as hydroxide-exchange electrolytes are still in early stages of development.[33]

While PEM-URFCs seem to be the leading technology for long-term energy storage, widespread commercialization has been hindered due to relatively low RTEs and disappointing long-term durability at the required high current densities. As a result, they have only found success in niche applications such as unmanned, limited payload, or extra-terrestrial vehicles,[34] where their energy density reigned over batteries. One of the main challenges towards solving these limitations is to develop bifunctional electrodes for URFC operation due to the combination of fuel cell and electrolyzer in one unitized device. Generally speaking, PEM-URFCs can be operated in two different modes:

constant-electrode (CE) mode and constant-gas (CG) mode. In CE mode (Figure 1a), hydrogen oxidation reaction (HOR) and oxygen evolution reaction (OER) occur in one electrode while oxygen reduction reaction (ORR) and hydrogen evolution reaction (HER) occur in the other electrode. The advantage of CE mode operation is the separation of ORR and OER to different electrodes, giving more room for electrode and gas/liquid diffusion layers design to obtain better cell efficiency. The disadvantages come from a wider range of operating potential for both electrodes, which might lead to faster materials degradation, and the management of risk of mixing of H_2 and O_2(air) between switching of charging/discharging. In CG mode (Figure 1b), HOR/HER occurs in one electrode while ORR/OER occurs in the other electrode. The CG mode operation avoids mixing of H_2 and O_2(air), allowing faster switching between charging/discharging, albeit liquid water purging between charge and discharge is still necessary. However, two limiting reactions (ORR and OER) are combined in the same side of the cell, resulting in a confluence of cell inefficiencies. Regardless of the mode, bifunctional electrodes are essential for URFC operation, which would pose constrains of electrode design compared to traditional discrete fuel cell and electrolyzers. For example, while carbon-supported materials are routinely used in fuel cells, they cannot be used for URFCs on the OER supporting electrode as carbon corrosion occurs during electrolysis operation.[23] Therefore, researchers have focused on developing non-carbon supported catalysts with bifunctional features especially for oxygen catalysis in CG mode URFCs.[35] Ir and Pt supported by metal oxides (such as TiO_2) bifunctional catalysts have garnered a lot of attention since these platinum-group-metal (PGM) catalysts retain high activity for both OER and ORR, while metal-oxide supports show increased durability under highly acidic

and oxidative conditions encountered during water electrolysis.[36–39] However, to date, the metal oxide supported Ir and Pt based bifunctional electrodes for PEM-URFCs have not met expectations. As reviewed by Wang *et.al*,[24] the state-of-the-art PEM-URFCs performance has been disappointing with either low RTE (~30 to 40%) or low operating current density (< 500 mA cm^{-2}). Additionally, there is a lack of durability studies for PEM-URFCs although there are several studies that report URFC durability under accelerated-stress tests[14,40] focused on start/stop behavior. Therefore, AST cycles do not necessarily capture all cell-level component degradation over time and fail to answer key questions such as whether URFCs could adapt to wide range of charge-discharge timeframes under various working conditions. As an electrochemical device to harness intermittent renewable resources, a URFC needs to operate at different charge-discharge timescales, especially aiming for grid scale applications that store large quantities of energy and cycle infrequently, as H_2-based technologies would be more economically favorable in those scenario compared to other technologies.[41] However, the majority of URFC studies in literature were not able to achieve satisfying long-term and stable operation at reasonably high current densities.[23,24] Thus, to ensure the technical viability of URFCs at reasonable LCOS, high RTEs at high current densities and long-term durability under various working conditions needs to be achieved.

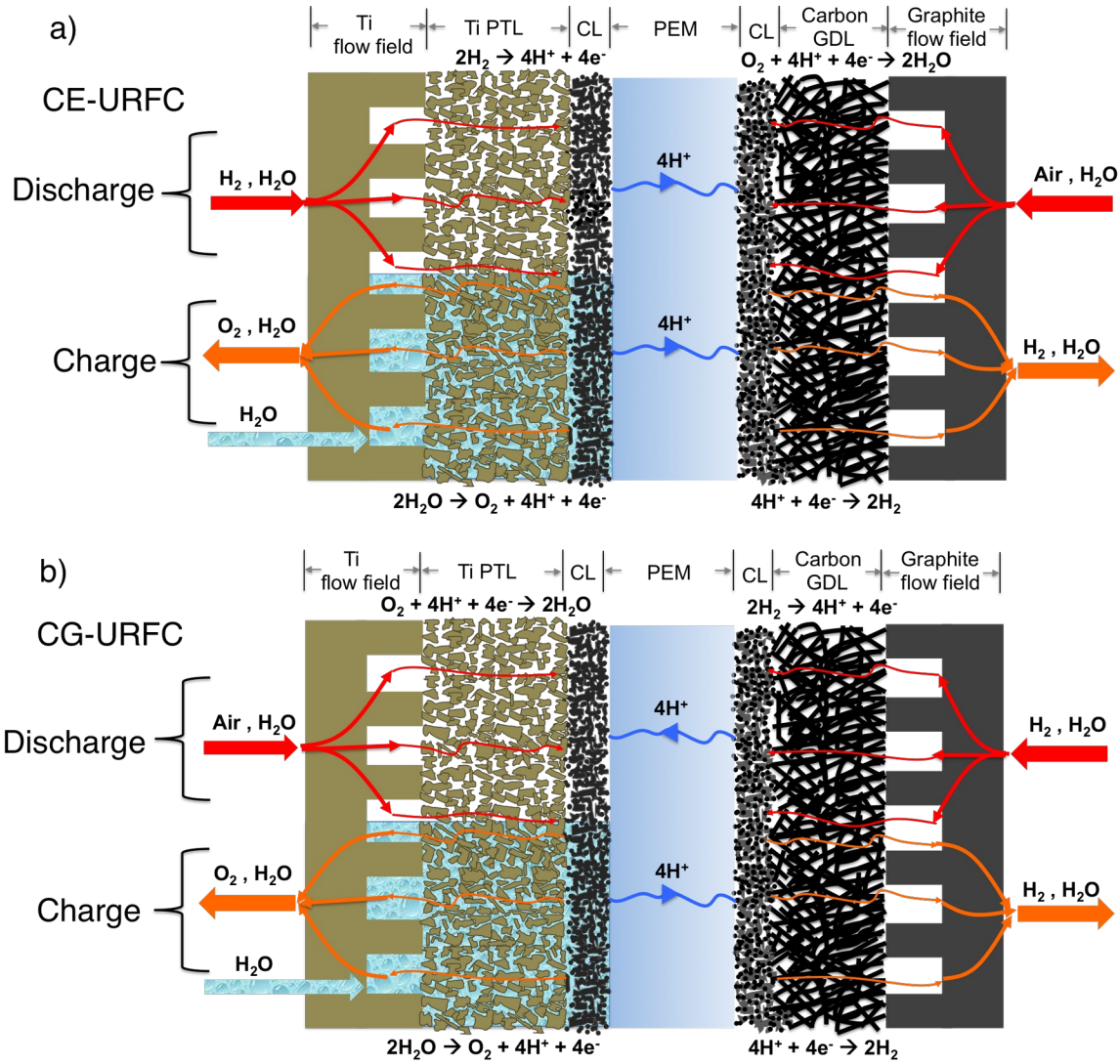

Figure 1. Schematic illustration of a) CE mode of URFC operation; b) CG mode of URFC operation. Red arrows indicate the mass flow during discharging (fuel cell) operation, while orange arrows indicate the mass flow during charging (electrolyzer) operation. The URFC devices used in this study consist of a platinized titanium (Ti) flow field, platinized Ti porous transport layer (PTL), proton exchange membrane (PEM), carbon based gas diffusion layer (GDL), graphite flow field and two catalyst layers at each side of the PEM.

Herein, we demonstrate our design and fabrication of a bifunctional electrode that breaks through the previously believed efficiency, performance, and durability barriers using commercially available Pt and Ir black electrocatalysts and other critical cells components,[24] thus demonstrating the power of hierarchical design and integration. Such

a PEM-URFC can deliver high RTEs at high current densities and high durability, *e.g.*, 56% RTE at 1000 mA cm^{-2} and over 500h of operation. The bifunctional electrode fabrication and system integration strategy can be applied to other complicated devices such as metal-air batteries and hydrocarbon electrochemical refineries.

Hierarchical Pt-Ir Electrode Fabrication

The strategy of mixing unsupported Pt-black and Ir-black catalysts to form a bi-functional electrode has been reported before;[42–46] however, none achieved high RTEs and/or stability. Since Pt black is just as active as Pt/C catalyst for ORR and HOR based on rotating-disk-electrode measurements,[47,48] and Ir black is the gold-standard catalyst for OER,[49] the missing performance of an unsupported Pt-Ir black electrode is not likely due to a lack of intrinsic catalyst activity. Instead, we hypothesize that it is the fabrication-dependent catalyst-layer structure and integration that leads to undesired mass-transport resistance and underutilized catalysts that hinder high URFC performance, especially at low catalyst loadings. Catalyst layers play a critical role in determining electrochemical-device performance, as they must ensure a triple percolated transport pathway (gas/liquid, ions, electron) and ensure an ideal reaction microenvironment at the catalyst site. For PEM-URFCs, the water and gas management becomes more challenging than discrete fuel-cell or electrolyzer technology, in particular the oxygen electrode requires both liquid water flow (during charging) and a humidified reactive gas without liquid water condensation (during discharging). In this work, we applied two electrode fabrication methods and related ink recipes including ultrasonic spray coating and doctor blading to create two types of Pt-Ir bifunctional electrodes for URFC operation. During ultrasonic

spray coating, very dilute, low viscosity ink is sprayed layer by layer onto the membrane substrate, whereas during doctor blading, more concentrated ink at higher viscosity is coated on the membrane substrate.[50] The detailed fabrication parameters were listed in the method section. The catalyst coated membrane (CCM) fabricated using doctor blading and ultrasonic spraying are denoted as DBCCM and SPCCM in the rest of text, respectively. The total PGM loading and Pt/Ir distribution were consistent between DBCCM and SPCCM MEAs, 0.8 mg/cm^2 total Pt metal loading and 0.5 mg/cm^2 total Ir metal loading, representing a total PGM reduction of 31% relative to discrete fuel cell and electrolyzer cell.[14]

Pt-Ir Electrode URFC Performance Evaluation

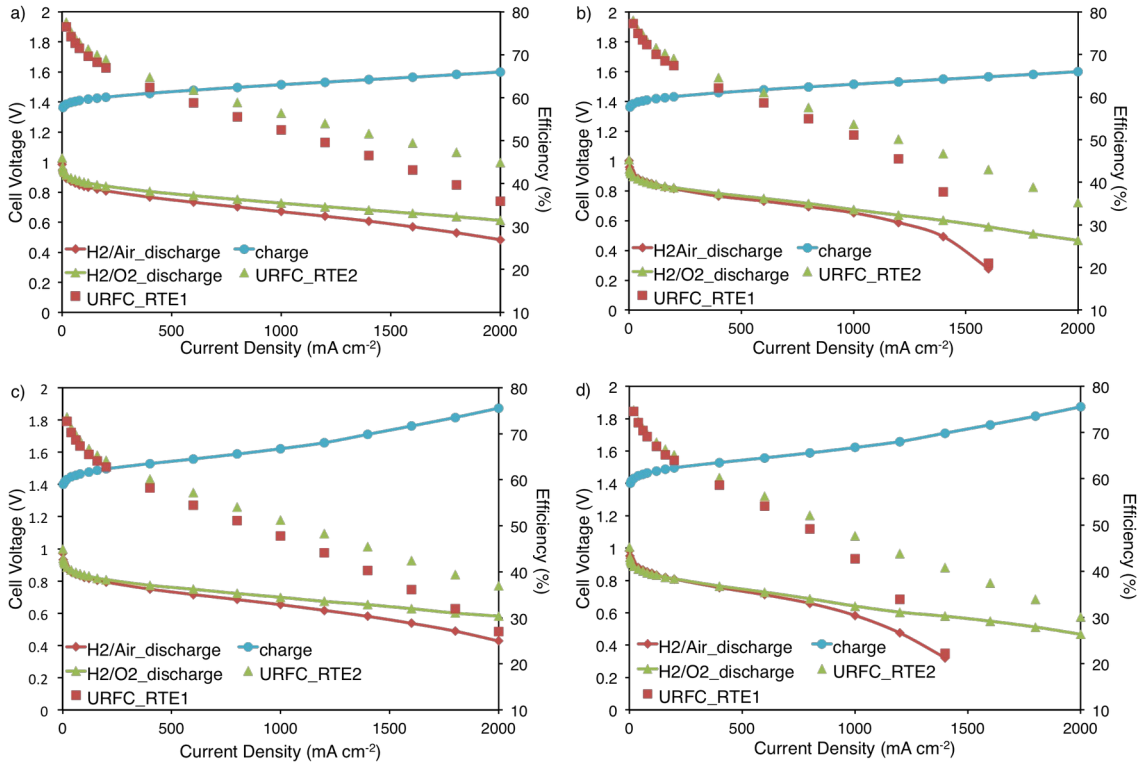

Figure 2 a), b) URFC charge/discharge polarization curves and RTEs evaluation using DBCCM under CE and CG mode, respectively; c), d) URFC charge/discharge polarization curves and RTEs evaluation using SPCCM under CE and CG mode, respectively. URFC-RTE1 and URFC-RTE2 are calculated when air and oxygen are used as oxidant at discharge mode, respectively. Nafion 212 was selected as membrane for all tests. Cells were operated at 80 °C. Data is presented without *iR* correction.

The URFC performance was evaluated by operating at charging (water electrolysis) mode followed by discharging mode (fuel cell) with O_2 and air feed, respectively. The charge-discharge polarization curves and round-trip efficiencies of the Pt-Ir electrode contained in URFC MEAs and hardware (titanium porous transport layer and titanium flowfield for the OER side of the cell) under both CE and CG mode are given in Figure 2. During charging, the *i-V* curve of DBCCM appears to be linear at

current density range of 500 - 2000 mA cm^{-2}, whereas the *i-V* curve of SPCCM shows two distinguishable slopes, indicating a higher mass transport resistance. During discharging, *i-V* curves of both DBCCM and SPCCM do not show significant mass transport limitation under CE mode, however, a clear mass transport region can be observed when air is used as oxidant under CG mode. The detailed voltage breakdown will be discussed in later sections. At 1000 mA cm^{-2} for both charging and discharging, DBCCM is able to achieve RTEs of 56.4% and 52.3% under CE-URFC (Figure 2a), and RTEs of 53.6% and 51.1% under CG-URFC (Figure 2b), with O_2 and air fed during discharging, respectively, which is the best-reported RTEs under both CE and CG operating mode for low-temperature URFCs (Table S1).[22,23] In the case of SPCCM, RTEs were calculated to be 51.3% and 47.8% under CE-URFC (Figure 2c), and 47.6% and 42.7% under CG-URFC (Figure 2d), with O_2 and air fed during discharging, respectively. It is clear that DBCCM achieves higher RTEs than SPCCM at the same testing condition under both CE and CG URFC operations. The result indicates that URFC performance and RTEs are sensitive to electrode fabrication method and subsequent catalyst-layer structure even at the same catalyst loading, which also hints that DBCCM could have more porous and less tortuous catalyst layer architecture compared to SPCCM. As more porous catalyst layer usually offers higher electrochemically active surface area indicated from Figure S1, showing DBCCM has one magnitude higher of double layer capacitance compared to SPCCM. Therefore, DBCCM possessed better catalyst utilization compared to SPCCM for ORR and OER due to enhanced creation of active surface area, leading to lower kinetic overpotential during charging (Figure S2a) and discharging (Figure S2b, S2c). Besides, as shown in Figure S2d - S2f, the mass-transport overpotential of DBCCM

is significantly lower compared to SPCCM for OER during charging (Figure S2d) and ORR during discharging (Figure S2e, S2f), respectively. The higher porosity and lower tortuosity of DMCCM could promote mass transport for both gaseous and liquid reactants and products, thus improve cell performance. The performance of DBCCM was further verified at 25 cm^2 by industrial partners, Nel Hydrogen and Ballard Power Systems, for charging and discharging at CG-URFC mode, respectively. As shown in Figure S3, the 25 cm^2 CCMs were able to achieve RTE of 51% at 1000 mA cm^{-2}, indicating the possibility of using current electrode design for large MEA and cell stack manufacture.

Pt-Ir Electrode URFC Stability

To investigate the feasibility and flexibility of URFCs for potential grid-energy-storage applications, we first conducted reversible operation of the DBCCM under CE-URFC mode via periodically switching between electrolysis and fuel cell at three different full charge/discharge timescales: daily, two-day, and bi-weekly (Figure 3a). The detailed description of switch between charge/discharge is shown in SI. For the first time, a tested CE-URFC achieved 600 h of continuous operation at 1000 mA cm^{-2} with only 20 mV of voltage loss, indicating well-retained RTEs (electricity to hydrogen to electricity) over charge/discharge cycles and very good operation flexibility under different working conditions. The performance decay could come from possible catalysts degradation as indicated from the ultra-small-angle X-ray scattering results (Figure S4), which show a slight particle size reduction after stability tests. Ex-situ accelerated stress tests were conducted on rotating disk electrode to further probe this observation. The results (Figure

S5) show that the degradation was more likely to come from Pt catalyst instead of Ir catalyst due to the wide operating voltage window of CE-URFC. Another test was also conducted to study the stability of unsupported Pt-Ir electrode under CG-URFC mode. To maintain better RTEs overtime, current densities of 1000 and 500 mA cm^{-2} were examined for charging and discharging, respectively. Reversible operation between two cycles of two-days charging followed by four-days discharging and one cycle of three-days charging followed by six-days discharging were conducted (Figure 3b). During 500 h of charge/discharge cycling, there was negligible voltage degradation and thus well-retained RTEs. Voltage oscillations noticed during discharging under CG mode were mostly likely due to the use of PTL as the gas-diffusion medium, leading to possible intermittent flooding issue. The voltage breakdown and performance analysis are shown in later sections. Overall, the rationally designed Pt-Ir black bifunctional electrode achieved excellent in-cell stability under both CE and CG operation mode and at much larger charge/discharge timescales compared to current LIB technologies, exhibiting a promising potential of URFC as a solution for long-term energy storage.

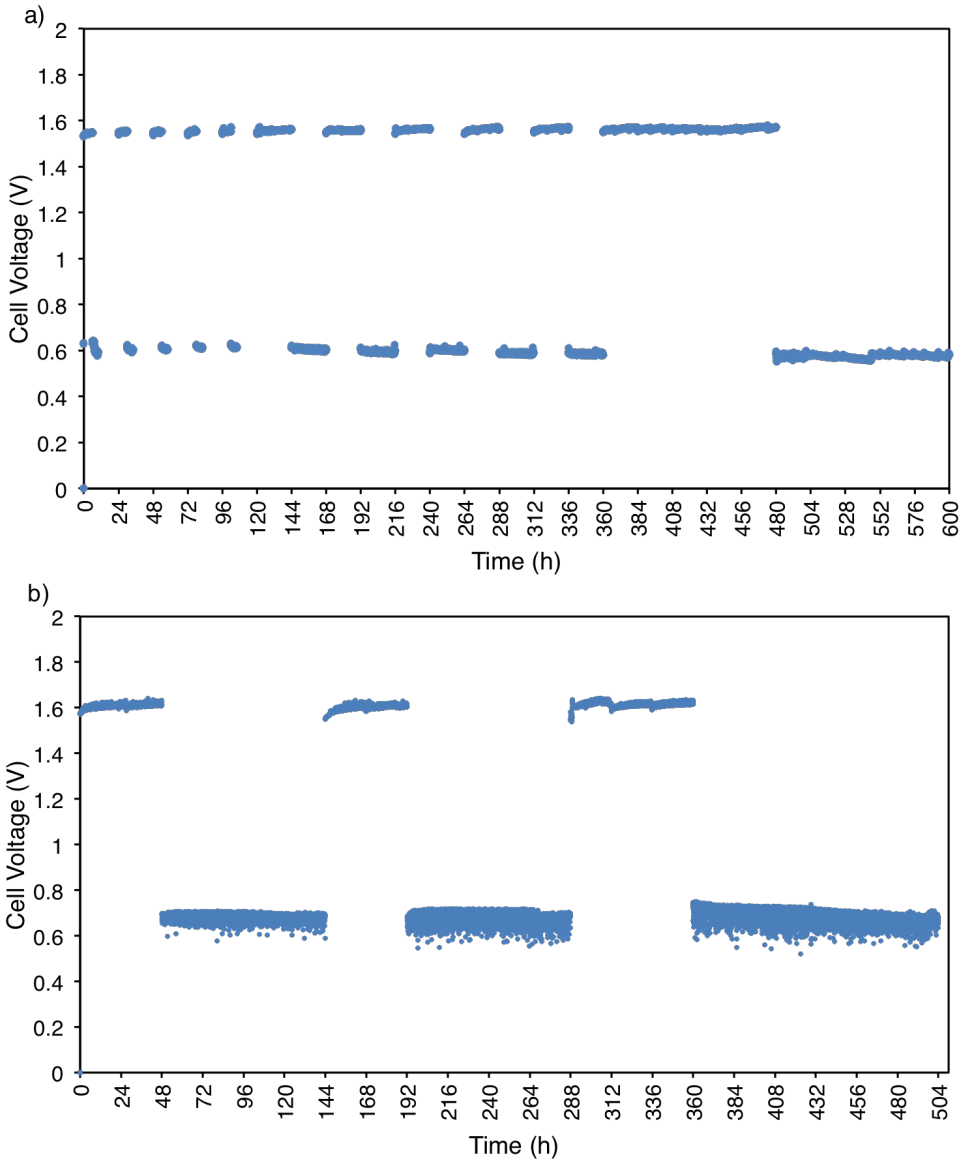

Figure 3. Longevity test of DBCCM at: a) CE mode in a 5 cm^2 MEA URFC device. Both charging and discharging were conducted at 1 A cm^{-2}; b) CG mode in a 5 cm^2 MEA URFC device. Charging and discharging were conducted at 1 A cm^{-2} and 0.5 A cm^{-2}, respectively. Air was fed to the cathode during discharging. Cell was maintained at 80 °C. Nafion 212 was selected as membrane. Cell was operated at 80 °C. Data is presented without *iR* correction.

URFC Voltage Breakdowns

Returning to the URFC performance in Figure 2, it is also interesting to note that operating CE-URFC achieved better RTEs compared to CG-URFC mode with both O_2

and air feed for both DBCCM (Figure 2a *vs.* Figure 2b) and SPCCM (Figure 2c *vs.* Figure 2d). This result is in agreement with our recent report by Regmi *et.al.*,[14] but without a detailed explanation; herein, we explore these observations further. Since OER always occurs on the electrode with Ir catalyst during charging, the RTE differences between CG-URFC and CE-URFC come from the performance difference during the discharging process. During discharge or fuel-cell mode, it's generally accepted that the sluggish ORR kinetics and poor cathode mass transport are limiting factors for cell performance,[51] therefore, whether ORR occurs on Pt/C electrode coupled with Sigracet 29BC GDL or on unsupported Pt-Ir electrode coupled with Ti PTL play a very important role in determining benefits and penalties of running CG-URFCs or CE-URFCs. Since all tests were conducted in the same device using the exact same membrane electrode assembly (MEA), the ohmic overpotential was measured to be very similar under all tested conditions (Figure S6). Therefore, we extracted the kinetic overpotential and mass-transport overpotential of DBCCM at both CE-URFC and CG-URFC mode when oxygen and air were used as oxidant (Figure 4), respectively. The detailed voltage breakdown process is listed in the supporting information. The ORR electrode kinetics were comparable between unsupported Pt-Ir electrode and Pt/C electrode, as the kinetic overpotential exhibited little difference between CE-URFC and CG-URFC during discharging under H_2/O_2 (Figure 4a) and H_2/Air (Figure 4b). The performance difference between CE-URFC and CG-URFC more likely stems from mass transport during discharging. As shown in Figure 4c and 4d, the mass-transport overpotential was significantly higher in CG mode than in CE mode, indicating that conventional carbon based GDL coupled with carbon-supported catalyst layer had superior mass transfer

compared to Pt-Ir black electrode coupled with Ti PTL. This is probably due to the fact that traditional carbon paper based GDL with micro porous layer and Pt/C catalyst layer have a more open structure and better-controlled hydrophobicity compared to Ti PTL and unsupported catalyst layer, which is more favorable for the gaseous reactant and liquid-product mass transport. A discharge performance comparison of DBCCM under CG mode operation between using carbon based GDL and Ti PTL is shown in Figure S7. The result indicates CG-URFC performance could be further improved with proper PTL design by mimicking the properties of carbon GDL. It is also interesting to note that the differences in mass-transport overpotential between CE-URFC and CG-URFC under H_2/O_2 (Figure 4c) are significantly lower than that under H_2/air (Figure 4d) especially at high current densities). For example, at the same current density of 1600 mA cm^{-2}, the mass-transport difference between CE-URFC and CG-URFC under H_2/O_2 is about 89 mV while it is 299 mV under H_2/air. This is probably because the Ti PTL (254 microns) is about 40% thicker than Sigracet 29BC GDL (177 microns), which enhances the diffusion length of oxygen in air, as previous studies have shown that the ratio of GDL thickness to the extent of the land is critical to the effective utilization of the catalyst in low O_2 concentration feed of PEMFC.[52] The high mass-transport overpotential under CG mode with air feed was further studied by mathematical modeling. The model is well calibrated based on the experimental data (Figure 4e). The breakdown shows the reactant transport in PTL has significant impact on the overall mass-transport overpotential, especially at medium to low current densities (Figure 4f). For example, it constitutes about 78.5% of the total mass-transport overpotential at a current density of 1000 mA cm^{-2}. As air feed URFC operation is a more practical choice, the above result indicates a thinner PTL and

tailored hydrophobicity could potentially help improve RTEs for future CG-URFC design.

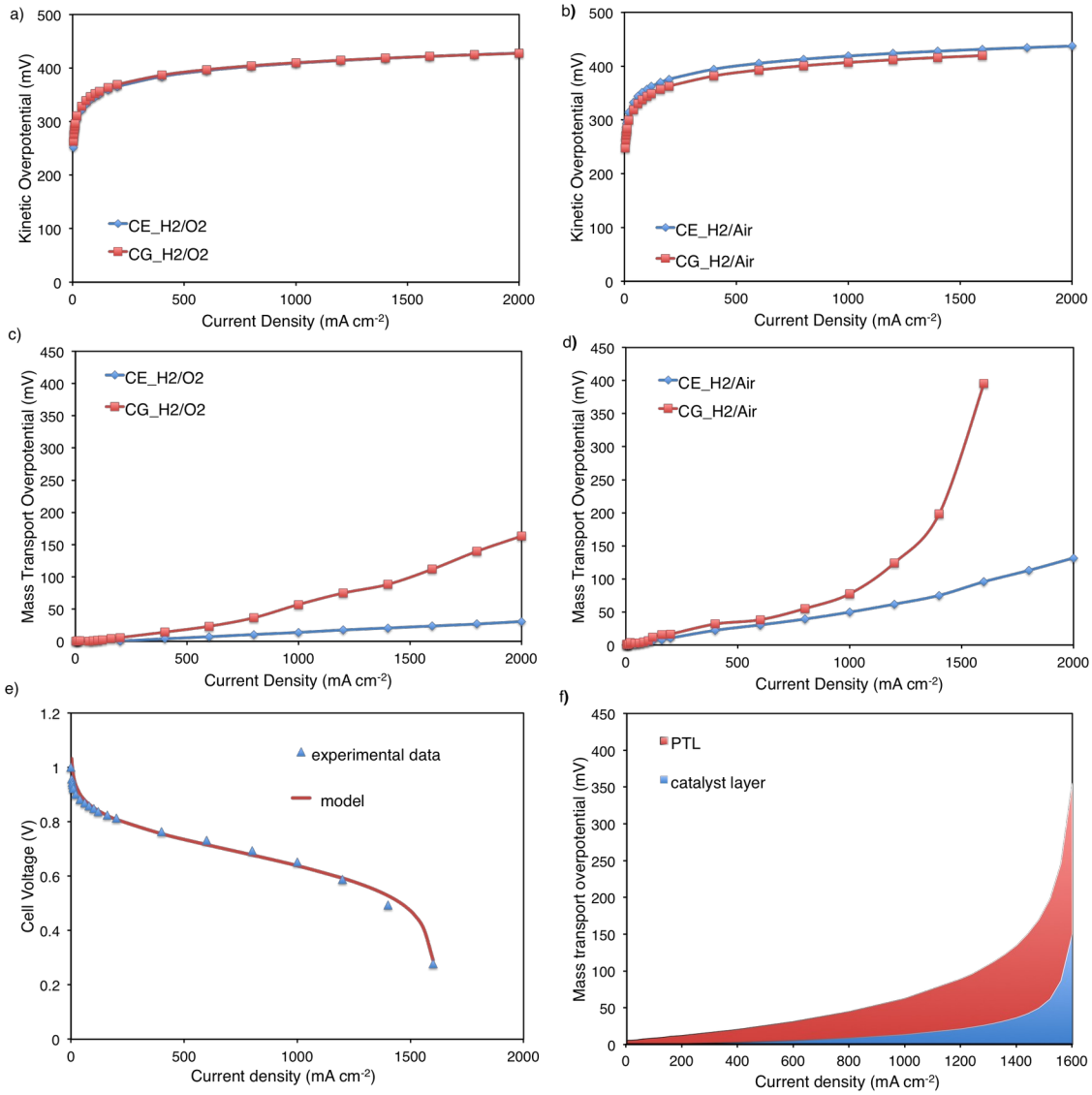

Figure 4. a), b) Kinetic overpotential of DBCCM under CE and CG mode when oxygen and air are used as oxidant for fuel cell, respectively; c), d) Mass transport overpotential of DBCCM under CE and CG mode when oxygen and air are used as oxidant for fuel cell, respectively; e) model calibration against experimental CG-URFC discharge polarization curve under air feed; f) mass-transport overpotential breakdown under CG-URFC discharge mode with air feed.

Pt-Ir Electrode Structural Analysis

To further investigate the structural properties of the DBCCM, scanning electron microscopy (SEM) and focused ion beam-scanning electron microscopy (FIB-SEM) were performed. As shown in Figure 5a, the DBCCM has a smooth and intact surface without visible cracking. The 3D microscopic structure of the Pt-Ir electrode (Figure 5b) is created by reconstructing a series of slice-view images obtained using FIB-SEM. The catalyst layer exhibits a very porous structure with interconnected pore channels that are well aligned with each other in vertical direction (Figure 5c). This is likely due to the doctor-blading fabrication process, wherein solvents vaporize when ink touches the hot substrate surface, and then transfer from the bottom side to the topside of catalyst layer, therefore creating interconnected porous structures, which should reduce catalyst-layer tortuosity. As a result, the solid phase (catalyst + ionomer) is also vertically connected (Figure 5d). By comparison, the SPCCM though shows a smooth surface morphology (Figure S8a), is featureless in terms of spatial distribution of pore and solid phase within the catalyst layer (Figure S8b-S8d). Thanks to the unique catalyst layer formation mechanism, even using unsupported Pt and Ir catalysts, the DBCCM has a porosity of 36.4%, which are much higher than the SPCCM of 29.3%. The tortuosity factor[53] of the Pt-Ir electrode was calculated using the TauFactor MATLAB plugin[54] which compares the steady-state diffusive flow through the measured pore network, which is based on microstructural image data, to that through a fully dense control volume of the same size and fluidic conditions.[54] The tortuosity factors accounting for not only the additional path length but also its change in the velocity of a species when migrating through a porous

structure, are evaluated at transverse, lateral and axial directions, which correspond to direction 1, 2, and 3 in Figure 5e, respectively. The DBCCM has lower tortuosity factors in all three directions compared to SPCCM (Figure 5f), in particular at the transverse direction. Besides, the flux density of DBCCM at steady state shows more transport pathways are provided at transverse direction compared to SPCCM (Figure S9 *vs.* Figure S10), therefore indicating a better catalyst layer utilization and lower mass transport resistance. The pore size distribution comparison (Figure S11) between the DBCCM and SPCCM indicates that a higher volume fraction in secondary pore range (around 10-40 nm)[55] helps the gaseous transport of reactants and products during URFC operation. The structural features of high porosity and low tortuosity factor sufficiently explain the superiority of DBCCM in enhancing catalyst utilization and reducing mass transport resistance for URFC operation. Besides, the doctor blading process can efficiently reduce electrode manufacture time even at large scale while fabricating electrodes with better RTEs for URFCs compared to the spraying method, therefore could potentially improve the overall LCOS based on our previous technical-economic analysis.[14]

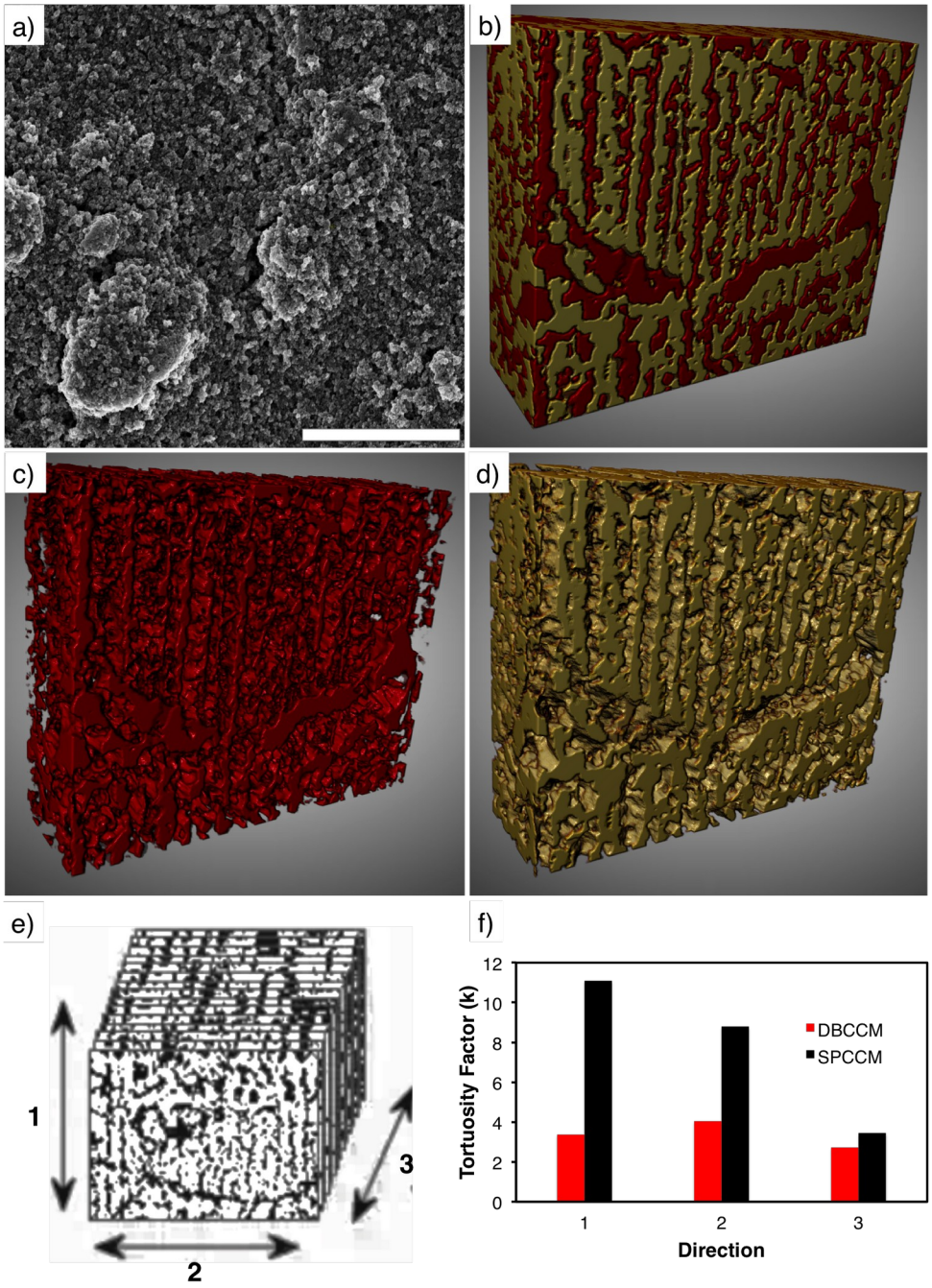

Figure 5. a) SEM image of the DBCCM, scale bar 5 µm; b) The reconstructed 3D Pt-Ir catalyst layer structure of DBCCM; c)-d) corresponded pore and solid 3D structures within the catalyst layer, respectively. The stack size is 5.57*4.61*1.2 µm. The total volume is 30.78 μm^3, total void volume is 11.21 μm^3. e) the three directions that tortuosity factors are obtained; f) comparison of tortuosity between DBCCM and SPCCM.

Conclusions

In summary, we utilized a hierarchical approach in design and optimization of the bifunctional catalyst layer to demonstrate PEM-URFC with the state-of-the-art round-trip efficiencies (RTEs) at high current densities and excellent long-term stable operation under both constant-electrode (CE) and constant-gas (CG) operation modes. The optimized Pt-Ir black electrode achieves RTEs of 56% and 53% under CE and CG mode, respectively, while operating at 1000 mA cm^{-2}. URFCs under both CE and CG mode were able to operate continuously for over 500 h with negligible degradation. We emphasize that at 2000 mA cm^{-2}, a surprising 45% RTE was achieved. The porosity and tortuosity of unsupported Pt-Ir catalyst layer played an important role in determining the URFC RTEs. Open and direct transport pathways enabled by more porous and less tortuous catalyst layers led to better catalyst utilization and lower mass transport resistance. The result indicates that developing electrocatalysts with bifunctional features may not be necessary but are still considered the holy grail. Instead, a well-designed catalyst layer with mixture of different catalyst dedicated to each of the fuel cell and electrolyzer half reaction could also achieve excellent URFC performance, and durability at a total PGM loading reduction of 31% compared to discrete systems. The performance analysis between CE and CG mode URFC indicated that mass transport was the critical factor limiting the CG URFC performance. The thick PTL may lead to extended O_2 diffusion length, underutilizes catalyst layer under the land and possible flooding during discharging. This work shows that URFCs can be performance-competitive with other long-duration or grid-scale energy-storage technologies and have a promising future; we

are taking next steps for stack design and scaleup toward the commercialization roadmaps.

Acknowledgements

The authors acknowledge the Department of Energy – Office of Energy Efficiency and Renewable Energy - Fuel Cell Technologies Office (DOE-EERE-FCTO) and program managers Greg Kleen and Dimitrios Papageorgopoulos for funding under Contract Number DE-AC02-05CH11231. Work at the Molecular Foundry was supported by the Office of Science, Office of Basic Energy Sciences, of the U.S. Department of Energy under Contract No. DE-AC02-05CH11231. Use of the Advanced Photon Source (APS), an Office of Science user facility operated by Argonne National Laboratory, is supported by the U.S. Department of Energy, Office of Science, Office of Basic Energy Sciences, under Contract No. DE-AS02-06CH11357. The authors would like to thank Jan Ilavsky and Ivan Kuzmenko of the X-ray Science Division, beamline 9-ID, of the APS. Z.T. would like to thank the support by the U.S. Department of Energy, Office of Science, Office of Workforce Development for Teachers and Scientists, Office of Science Graduate Student Research (SCGSR) program. The SCGSR program is administered by the Oak Ridge Institute for Science and Education (ORISE) for the DOE. ORISE is managed by ORAU under contract number DE-SC0014664. All opinions expressed in this paper are the author's and do not necessarily reflect the policies and views of DOE, ORAU, or ORISE. We thank NEL/Proton OnSite for providing Ti PTLs. We also thank Marcelo Carmo from Forschungszentrum Jülich for the inspiration to use viscous ink. N.D. and A.Z.W. conceived the project and secured funding; X.P., Z.T., N.D., J.F. and

Y.N.R. designed and conducted the electrode fabrication and testing experiments; C.C. and D.B. performed 25 cm^2 cell testing; J.L. performed the multiscale modeling, Y.Q.Z., X.X.P. and M.S. conducted FIB-SEM experiments. N.K. and D.J.M conducted the scattering experiments. X.P. and N.D. composed the manuscript, and all the authors edited it.

Conflicts of Interest
The authors declare no conflicts of interests.

References:

1. (U.S. Department of Energy). *International Energy Outlook 2019 with Projections to 2050*. (2019).
2. Hannan, M. A. *et al.* Power electronics contribution to renewable energy conversion addressing emission reduction : Applications , issues , and recommendations. *Appl. Energy* **251**, 113404 (2019).
3. Gur M. Turgut. Review of electrical energy storage technologies, materials and systems : challenges and prospects for large-scale grid storage. *Energy Environ. Sci.* **11**, 2696–2767 (2018).
4. ENERGY, I. *Global Energy and CO2 Status Report*. (2019).
5. Jenkins, J. D., Luke, M. & Thernstrom, S. Getting to Zero Carbon Emissions in the Electric Power Sector. *Joule* **2**, 2498–2510 (2018).
6. Sepulveda, N. A. *et al.* The Role of Firm Low-Carbon Electricity Resources in Deep Decarbonization of Power Generation. *Joule* **2**, 2403–2420 (2018).
7. Dunn, B., Kamath, H. & Tarascon, J. Electrical Energy Storage for the Grid : A Battery of Choices. *Science.* **334**, 928–936 (2011).
8. Schmidt, O., Melchior, S., Hawkes, A. & Staffell, L. Projecting the Future Levelized Cost of Electricity Storage Technologies. *Joule* **3**, 81–100 (2019).
9. Zimmerman, H. A. Self-Discharge Losses in Lithium-Ion Cells. *IEEE AESS Syst. Mag.* (2004).
10. Pellow, M. A., Emmott, C. J. M., Barnhart, J. & Benson, S. M. Hydrogen or batteries for grid storage ? A net energy analysis †. *Energy Environ. Sci.* **8**, 1938–1952 (2015).
11. P, L. *et al.* Recent developments in organic redox flow batteries : A critical review. *J. Power Sources* **360**, 243–283 (2017).

12. Perry, M. L., Perry, M. L. & Weber, A. Z. Advanced Redox-Flow Batteries : A Perspective. *J. Electrochem. Soc.* **1**, A5064–A5067 (2016).
13. Weber, A. Z. *et al.* Redox flow batteries : a review. *J. Appl. Electrochem.* **41**, 1137–1164 (2011).
14. Regmi, Y. N. *et al.* A low temperature unitized regenerative fuel cell realizing 60% round trip efficiency and 10 000 cycles of durability for energy storage applications. *Energy Environ. Sci.*, 2020, **13**,2096-2105
15. Kilner, J. A. & Skinner, S. J. Development of oxygen electrodes for reversible solid oxide fuel cells with scandia stabilized zirconia electrolytes. *Solid State Ionics* **192**, 501–504 (2011).
16. Wendel, C. H. & Braun, R. J. Design and techno-economic analysis of high efficiency reversible solid oxide cell systems for distributed energy storage. *Appl. Energy* **172**, 118–131 (2016).
17. Nguyen, V. N., Fang, Q., Packbier, U. & Blum, L. Long-term tests of a Julich planar short stack with reversible solid oxide cells in both fuel cell and electrolysis modes. *Int. J. Hydrogen Energy* **38**, 4281–4290 (2013).
18. Jensen, S. H. *et al.* Large-scale electricity storage utilizing reversible solid oxide cells combined with underground storage of CO2 and CH4. *Energy Environ. Sci.* **8**, 2471–2479 (2015).
19. Elangovan, S., Hartvigsen, J. J. & Frost, L. J. Intermediate Temperature Reversible Fuel Cells. *Appl. Ceram. Technol.* **118**, 109–118 (2007).
20. Wendel, C. H., Gao, Z., Barnett, S. A. & Braun, R. J. Modeling and experimental performance of an intermediate temperature reversible solid oxide cell for high-efficiency, distributed-scale electrical energy storage. *J. Power Sources* **283**, 329–342 (2015).
21. Duan, C. *et al.* Highly efficient reversible protonic ceramic electrochemical cells for power generation and fuel production. *Nat. Energy* **4**, 230–240 (2019).
22. Wang, Y., Leung, D. Y. C., Xuan, J. & Wang, H. A review on unitized regenerative fuel cell technologies , part B: Unitized regenerative alkaline fuel cell , solid oxide fuel cell, and micro fluidic fuel cell. *Renew. Sustain. Energy Rev.* **75**, 775–795 (2017).
23. Sadhasivam, T. *et al.* A comprehensive review on unitized regenerative fuel cells: Crucial challenges and developments. *Int. J. Hydrogen Energy* 1–19 (2016) doi:10.1016/j.ijhydene.2016.10.140.
24. Wang, Y., Leung, D. Y. C., Xuan, J. & Wang, H. A review on unitized regenerative fuel cell technologies , part-A : Unitized regenerative proton exchange membrane fuel cells. *Renew. Sustain. Energy Rev.* **65**, 961–977 (2016).
25. Badwal, S. P. ., Giddey, S., Munnings, C. & Kulkarni, A. Review of Progress in High Temperature Solid Oxide Fuel. *J. Aust. Ceram. Soc.* **50**, 23–37 (2014).
26. Comparison of Fuel Cell Technologies. *https://www.energy.gov/eere/fuelcells/comparison-fuel-cell-technologies*.
27. Wang, Q. *et al.* Transition from core-shell to janus segregation pattern in AgPd nanoalloy by Ni doping for the formate oxidation. *Appl. Catal. B Environ.* **270**, 118861 (2020).

28. Guo, L. *et al.* Surface reconstruction of AgPd nanoalloy particles during the electrocatalytic formate oxidation. *Nanoscale* **12**, 3469–3481 (2020).
29. Zhang, N., Chen, F. & Guo, L. Catalytic activity of palladium-doped silver dilute nanoalloys for formate oxidation from a theoretical perspective †. *Phys.Chem.Chem.Phys* **21**, 22598–22610 (2019).
30. Wang, J. *et al.* In situ high-potential-driven surface restructuring of ternary AgPd–Ptdilute aerogels with record-high performance improvement for formate oxidation electrocatalysis. *Nanoscale* **11**, 14174 (2019).
31. Tang, Q., Chen, F., Jin, T. & Guo, L. Alloying in inverse CeO 2 / Pd nanoparticles to enhance the electrocatalytic activity for the formate oxidation reaction †. *J. Mater. Chem. A* **7**, 22996–23007 (2019).
32. Wang, Q. *et al.* Nanoalloying effects on the catalytic activity of the formate oxidation reaction over AgPd and AgCuPd aerogels. *J. Mater. Chem. A* **7**, 16122 (2019).
33. Dekel, D. R. Review of cell performance in anion exchange membrane fuel cells. *J. Power Sources* **375**, 158–169 (2018).
34. Mitlitsky, F., Myers, B. & Weisberg, A. H. Regenerative Fuel Cell Systems. *Energy and Fuels* **12**, 56–71 (1998).
35. Pettersson, J., Ramsey, B. & Harrison, D. A review of the latest developments in electrodes for unitised regenerative polymer electrolyte fuel cells. *J. Power Sources* **157**, 28–34 (2006).
36. Huang, S. ., Ganesan, P., Jung, W. S., Cadirov, N. & Popov, B. N. Development of Supported Bifunctional Oxygen Electrocatalysts with High Performance for Unitized Regenerative Fuel Cell Applications. *ECS Trans.* **33**, 1979–1987 (2010).
37. Kong, F. *et al.* Preparation of Pt/Irx(IrO2)10−x bifunctional oxygen catalyst for unitized regenerative fuel cell. *J. Power Sources* **210**, 321–326 (2012).
38. Zhang, T. *et al.* Shape-tunable Pt-Ir alloy nanocatalysts with high performance in oxygen electrode reactions. *Nanoscale* **9**, 1154–1165 (2017).
39. Won, J. *et al.* PtIr/Ti4O7 as a bifunctional electrocatalyst for improved oxygen reduction and oxygen evolution reactions. *J. Catal.* **358**, 287–294 (2018).
40. Zhang, Y., Wang, C., Wan, N. & Mao, Z. Deposited RuO2–IrO2/Pt electrocatalyst for the regenerative fuel cell. *Int. J. Hydrogen Energy* **32**, 400–404 (2007).
41. Davis, S. J. *et al.* Net-zero emissions energy systems. *Science (80-.).* 1419 (2018) doi:10.1126/science.aas9793.
42. Jung, H., Park, S. & Popov, B. N. Electrochemical studies of an unsupported PtIr electrocatalyst as a bifunctional oxygen electrode in a unitized regenerative fuel cell. *J. Power Sources* **191**, 357–361 (2009).
43. Ho-Young Jung, Prabhu Ganesan, and B. N. P. Development of High Durability Bi-functional Oxygen Electrode for Unitized Regenerative Fuel Cell (URFC). *ECS Trans.* 1261–1269 (2009).
44. Yim, S. *et al.* Optimization of bifunctional electrocatalyst for PEM unitized regenerative fuel cell. *Electrochim. Acta* **50**, 713–718 (2004).
45. Ioroi, T., Kitazawa, N., Yasuda, K. & Yamamoto, Y. Iridium Oxide/Platinum Electrocatalysts for Unitized Regenerative Polymer Electrolyte Fuel Cells Iridium

Oxide/Platinum Electrocatalysts for Unitized Regenerative Polymer Electrolyte Fuel Cells. *J. Electrochem. Soc.* 2018–2022 (2000).
46. Ioroi, T., Yasuda, K., Siroma, Z., Fujiwara, N. & Miyazaki, Y. Thin film electrocatalyst layer for unitized regenerative polymer electrolyte fuel cells. *J. Power Sources* **112**, 583–587 (2002).
47. Lim, B. *et al.* Pd-Pt Bimetallic Nanodendrites with High Activity for Oxygen Reduction. *Science.* **324**, 1302–1306 (2009).
48. Li, F., Gao, X., Li, S., Chen, Y. & Lee, J. Thermal decomposition synthesis of functionalized PdPt alloy nanodendrites with high selectivity for oxygen reduction reaction. *NPG Asia Mater.* e219 (2015) doi:10.1038/am.2015.108.
49. Mccrory, C. C. L., Jung, S., Peters, J. C. & Jaramillo, T. F. Benchmarking Heterogeneous Electrocatalysts for the Oxygen Evolution Reaction. *J. Am. Chem. Soc.* 16977–16987 (2013) doi:10.1021/ja407115p.
50. Hatzell, K. B., Dixit, M. B., Berlinger, S. A. & Weber, A. Z. Understanding inks for porous-electrode formation. *J. Mater. Chem. A* **5**, 20527–20533 (2017).
51. Gasteiger, H. A., Kocha, S. S., Sompalli, B. & Wagner, F. T. Activity benchmarks and requirements for Pt, Pt-alloy, and non-Pt oxygen reduction catalysts for PEMFCs. *Appl. Catal. B Environ.* **56**, 9–35 (2005).
52. Benziger, J., Kimball, E., Mejia-ariza, R. & Kevrekidis, I. Oxygen Mass Transport Limitations at the Cathode of Polymer Electrolyte Membrane Fuel Cells. *Aiche J.* **57**, (2011).
53. Tjaden, B., Brett, D. J. L. & Shearing, P. R. Tortuosity in electrochemical devices: a review of calculation approaches. *Int. Mater. Rev.* **63**, 47–67 (2018).
54. Cooper, S. J., Bertei, A., Shearing, P. R., Kilner, J. A. & Brandon, N. P. TauFactor : An open-source application for calculating tortuosity factors from tomographic data. *SoftwareX* **5**, 203–210 (2016).
55. Electrochem, M. E. J., Soc, E. & Eikerling, M. Water Management in Cathode Catalyst Layers of PEM Fuel Cells : A Structure-Based Model PEM Fuel Cells. *J. Electrochem. Soc.* **153**, E58–E70 (2006).